

Design of inverse controller with cross-coupling suppression for UPFC series converter

Abstract—The power flow control problem of a transmission line equipped with a Universal Power Flow Controller is investigated. Two controllers for the series converter of a UPFC are proposed. Dynamic or static model inverses are used to linearize control and suppress cross-coupling dynamics. Both controllers realize first order step responses with arbitrary time constant and cross-coupling suppression. Main benefits of these controllers are low controller complexity, minimal required system parameter knowledge and first order system behavior with arbitrary time constant. Controller complexity is no more than two parallel PI controllers for the steady-state inverse controller, or four for the dynamic inverse controller. Cross-coupling suppression performance of both controllers depends only on knowledge of inductance-resistance ratio of transmission line. Simulation results at 1 kHz demonstrate cross-coupling suppression and first order behavior. Control bandwidth allows damping of inter-area oscillations.

I. INTRODUCTION

A GROWING demand for electrical energy in Europe is not met by an equal growth of the transmission system. Existing transmission lines were designed for local delivery and interconnection lines were designed for emergency support. As the European electricity grid now hosts a liberalized energy market, these lines now guide international power flows. The system frequently reaches its stability limit and effects of local faults spread wider, as control options are exploited to maximize profit. New, flexible tools to control power flows on the transmission network are topic of ongoing research.

Flexible Alternative Currents Transmission System (FACTS) is a family of power electronic devices capable of dynamically controlling power systems. The Universal Power Flow Controller (UPFC) is the most versatile of devices in the FACTS concept, being able to control three basic variables of a transmission line, namely transmission voltage, line impedance and phase angle. In formula 1, active and reactive power P, Q transported by an ideal purely inductive transmission line are given, in function of sending and receiving end voltages V_S, V_R , line impedance X and phase angle ρ . This is a commonly used model for overhead lines, whose impedance is mainly inductive. As a UPFC can control the sending end voltage V_S , phase angle ρ and line impedance X , it can adequately control active and reactive power flow on a transmission line.

$$P = \frac{V_S \cdot V_R \cdot \sin \rho}{X} \quad Q = \frac{V_S^2 - V_S \cdot V_R \cdot \cos \rho}{X} \quad (1)$$

A UPFC consists of two AC-DC converters, connected back to back with their DC side. The AC sides are connected to the transmission line, one in shunt, the other in series of the line by means of a coupling transformer. In Figure 1, a one wire schematic of a UPFC is depicted. Voltages V_P and V_C

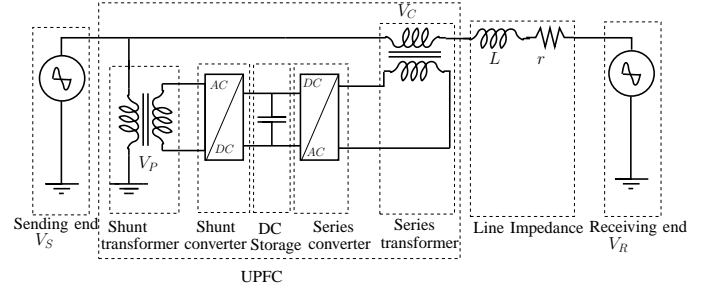


Fig. 1. One-wire schematic of transmission line equipped with UPFC

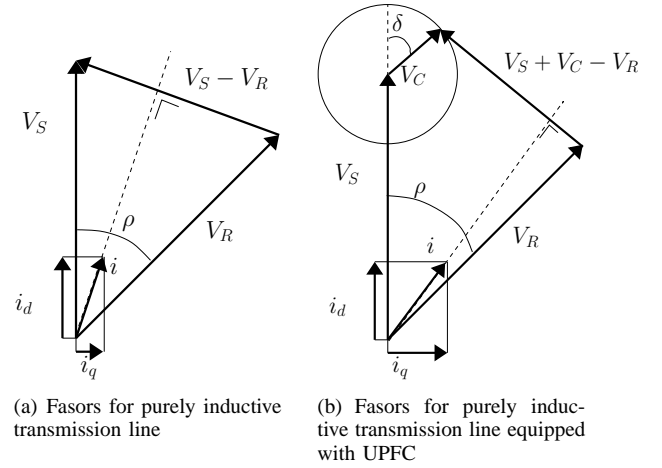


Fig. 2. Fazor representation of effect of UPFC on current i , component i_d, i_q and thereby on active and reactive power

represent shunt and series converter voltages of the UPFC. L and r represent inductance and resistance of the overhead line. Both converters can independently absorb and generate reactive power, and active power can flow in both directions between shunt and series converter. The DC energy storage serves as a buffer for momentary active power flow imbalances between converters. This allows the series converter to inject an arbitrary series voltage, realizing power flow control and impedance compensation, while the shunt converter balances the active power flow and injects reactive power for voltage stabilization of the sending end. Converters used for UPFC's are typically voltage sourced converters, having a capacitor as (limited) DC energy storage.

The effect of a UPFC on active and reactive power flow is shown in fazor representation in Figure 2. For simplicity, the resistive component of the line impedance is neglected. Results and conclusions are not affected by this. In Figure 2(a), sending and receiving voltages V_S, V_R are shown with phase ρ , and a current i , which is perpendicular to the difference $V_S -$

V_R because of neglecting the resistance of the line. Current i can be decomposed into direct and quadrature components i_d, i_q , representing the active and reactive current, and thereby the active and reactive power. For a given transmission line impedance X , voltages V_S, V_R and phase angle ρ , active and reactive power flow are fixed. In Figure 2(b), the injected series voltage V_C , with phase angle δ to sending end voltage V_S , influences directly the difference $V_S + V_C - V_R$, resulting in control over the active and reactive power flow. The series converter will operate only in a certain amplitude boundary, represented by a circle. Considering this limitation, arbitrary combinations of i_d, i_q can be realized by controlling V_C and δ . The fasor representation is only useful for steady state solutions, since dynamics can not be represented.

In an attempt to summarize the evolution of UPFC control design for power flow control, the steps taken from direct control, over decoupling control to cross-coupling control from direct and quadrature series injected voltages V_{Cd}, V_{Cq} to active and reactive power P, Q are a first important milestone [1], [2]. These controllers were based on PI control structures, and did not intrinsically rely on system parameters. A second step was taken by using cross-coupling control with direct control oscillation dampening [3], which enhanced performance. Further controllers increase controller complexity, leaving the full potential of PI based controllers unexplored. A next step introduced the instantaneous power concept, where current references were calculated based on instantaneous measurements of power, voltages and currents [4], [5], [6]. The final step was incorporating power source basic control and dynamics into the system model, to optimize damping of inter area oscillations. The obtained model is called the Philips-Heffron model of the power system and requires precise knowledge of numerous parameters of both transmission line and power sources. Controllers based on this model have high controller complexity [7], [8], [9], [10].

In this paper, two controllers for the series converter of a UPFC are proposed, maximizing the performance for controllers based on PI control structures. The controllers are based on a dynamic and steady-state model inverse of the power system. Exploiting system dynamics for control, controller complexity is limited to two parallel PI controllers for steady-state inverse controller, and four for dynamic inverse controller. First order system behavior with arbitrary time constant of the controlled system is realized. Cross-coupling of active and reactive power is suppressed, depending only on inductance/resistance ratio of the transmission line. The control of the shunt converter is not discussed in the remainder of this work as it is only used for voltage control at the sending end, and to maintain the power balance between shunt and series converter by energizing the DC capacitor. Section II constructs the dynamic and steady state models of a transmission line equipped with a UPFC. Section III present the design of the proposed dynamic and steady-state inverse controllers. To demonstrate robustness and insensitivity to measurement noise, an altered transmission line is used in simulation, with a mid-line load distorting the power flow equations and introducing different dynamics. Simulation results are proposed in Section IV. Conclusions are drawn in

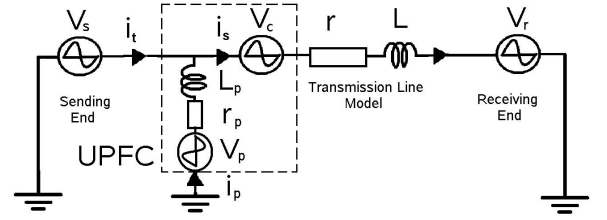


Fig. 3. Equivalent Circuit of UPFC system for currents

Section V.

II. MODELING OF UPFC POWER SYSTEM

The system used to model the effect of the UPFC on the transmission line is given in Figure 3 in one wire representation. Sending and receiving end power sources V_S, V_R are connected by transmission line r, L . The total current drawn from the sending end i_t consists of the current flowing through the line i_s and the current exchanged with the shunt converter i_p . Shunt transformer inductance and resistance are represented by L_p and r_p . Series transformer inductance and resistance are assumed negligible compared to transmission line impedance, and are therefore not represented in Figure 3.

Power sources V_S, V_R are assumed to be infinite, meaning that their amplitude and phase are not affected by changes in active or reactive power demand and also that no model dynamics originate from the power sources. This simplifies model construction and controller design. Assuming voltage support by the shunt converter of the UPFC to sending end power source V_S makes the assumption reasonable, while simulation will show the relative indifference of controller performance to the validity of this assumption for receiving end power source V_R .

The commonly accepted model used for the overhead transmission lines of lengths up to 50 km consists of a series inductance and resistance [11].

Connection transformers of series and shunt converters of the UPFC as in Figure 1 are not explicitly included in the mathematical model used for controller design. During simulation, the transformer dynamics are incorporated however. This simplifies model construction, and controller performance would not differ much.

The power on which the power flow control is based will be measured at sending end, meaning that it is formed by the current i_s and the receiving end voltage V_S . Since shunt converter current i_p is used for voltage support and DC energy storage balancing without influence on power flow, it is not necessary to further model it.

A. Dynamic model

Using the one wire model of Figure 3, differential equations that describe the current i_s in three phases can be formulated. Applying the Park transformation results in differential equations in dq space in equation 3. Applying the Laplace transformation results in transfer functions of the system, as in equation 4. Voltages V_d and V_q are introduced in equation 2 for notation simplicity. By substitution between the two transfer

functions of equation 4, equation 5 is obtained, where currents $i_{sd}(s), i_{sq}(s)$ are given in function of voltages $V_d(s)$ and $V_q(s)$.

$$\begin{aligned} V_d &= V_{sd} + V_{cd} - V_{rd} \\ V_q &= V_{sq} + V_{cq} - V_{rq} \end{aligned} \quad (2)$$

$$L \frac{\delta}{\delta t} \begin{bmatrix} i_{sd} \\ i_{sq} \end{bmatrix} = \begin{bmatrix} -r & \omega \cdot L \\ -\omega \cdot L & -r \end{bmatrix} \cdot \begin{bmatrix} i_{sd} \\ i_{sq} \end{bmatrix} + \begin{bmatrix} V_d \\ V_q \end{bmatrix} \quad (3)$$

$$\begin{aligned} \left(s + \frac{r}{L}\right) \cdot i_{sd} &= \omega \cdot i_{sq} + \frac{V_d}{L} \\ \left(s + \frac{r}{L}\right) \cdot i_{sq} &= -\omega \cdot i_{sd} + \frac{V_q}{L} \end{aligned} \quad (4)$$

By substitution between transfer functions in equation 4 the transfer functions of equation 5 can be obtained.

$$\begin{bmatrix} i_{sd}(s) \\ i_{sq}(s) \end{bmatrix} = \frac{1}{L} \cdot \begin{bmatrix} \left(s + \frac{r}{L}\right) & \omega \\ -\omega & \left(s + \frac{r}{L}\right) \end{bmatrix} \cdot \begin{bmatrix} V_d(s) \\ V_q(s) \end{bmatrix} \quad (5)$$

Active and reactive power at sending end are calculated as in equation 6.

$$\begin{aligned} P(s) &= V_{sd}(s) \cdot i_{sd}(s) + V_{sq}(s) \cdot i_{sq}(s) \\ Q(s) &= V_{sq}(s) \cdot i_{sd}(s) - V_{sd}(s) \cdot i_{sq}(s) \end{aligned} \quad (6)$$

As said before, no dynamics are related to the power sources' voltages, so in Laplace domain, power source voltages are constants. To simplify notation, it is assumed that by means of a phase locked loop the Park transformation is performed in phase with the sending end voltage, meaning that $V_{sq} = 0$. This results in 9.

$$\begin{aligned} P(s) &= P_0(V_s, V_r) + \Delta P(V_c(s)) \\ Q(s) &= Q_0(V_s, V_r) + \Delta Q(V_c(s)) \end{aligned} \quad (7)$$

$$\begin{aligned} P_0(V_s, V_r) &= V_{sd} \cdot \frac{((V_{sd} - V_{rd}) \cdot r - \omega \cdot L \cdot V_{rq})}{r^2 + (\omega \cdot L)^2} \\ Q_0(V_s, V_r) &= V_{sd} \cdot \frac{(V_{rq} \cdot r + \omega \cdot L \cdot (V_{sd} - V_{rd}))}{r^2 + (\omega \cdot L)^2} \end{aligned} \quad (8)$$

$$\begin{aligned} \Delta P(V_c(s)) &= +V_{cd}(s) \cdot \frac{V_{sd} \cdot (L \cdot s + r)}{(L \cdot s + r)^2 + (\omega \cdot L)^2} \\ &\quad + V_{cq}(s) \cdot \frac{V_{sd} \cdot \omega \cdot L}{(L \cdot s + r)^2 + (\omega \cdot L)^2} \\ \Delta Q(V_c(s)) &= +V_{cd}(s) \cdot \frac{V_{sd} \cdot \omega \cdot L}{(L \cdot s + r)^2 + (\omega \cdot L)^2} \\ &\quad - V_{cq}(s) \cdot \frac{V_{sd} \cdot (L \cdot s + r)}{(L \cdot s + r)^2 + (\omega \cdot L)^2} \end{aligned} \quad (9)$$

Both active and reactive power consist of a uncontrollable constant part, which is determined by power source voltages and line impedance, and a controllable dynamic part, determined by converter voltage, as explicited in equation 7. System dynamics are different for direct and cross-coupled control between P, Q and V_{Cd}, V_{Cq} . The dynamic controller to be designed will use the knowledge of these dynamics to compensate for them.

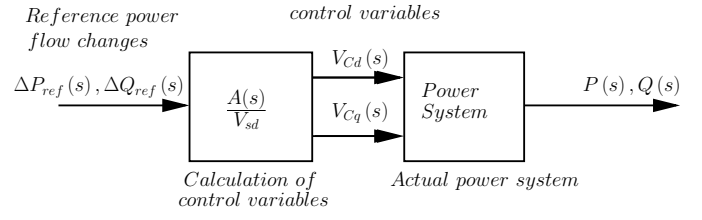


Fig. 4. Open Loop Control structure, where $A(s)$ is used to linearize control. Actual Power system dynamics may differ from those modeled

B. Steady state model

Applying the Final Value Theorem ($s \rightarrow 0$) to the dynamic system equations 7, the steady state solutions for power flow control can be found in equation 10.

$$\begin{aligned} P &= P_0(V_s, V_r) + \Delta P(V_c) \\ Q &= Q_0(V_s, V_r) + \Delta Q(V_c) \end{aligned} \quad (10)$$

$P_0(V_s, V_r)$ and $Q_0(V_s, V_r)$ are the same as in equation 8. $\Delta P(V_c)$ and $\Delta Q(V_c)$ can be found in equation 11

$$\begin{aligned} \Delta P(V_c) &= V_{cd} \cdot \frac{V_{sd} \cdot r}{r^2 + (\omega \cdot L)^2} + V_{cq} \cdot \frac{V_{sd} \cdot \omega \cdot L}{r^2 + (\omega \cdot L)^2} \\ \Delta Q(V_c) &= V_{cd} \cdot \frac{V_{sd} \cdot \omega \cdot L}{r^2 + (\omega \cdot L)^2} - V_{cq} \cdot \frac{V_{sd} \cdot r}{r^2 + (\omega \cdot L)^2} \end{aligned} \quad (11)$$

The controllable part of steady-state active and reactive power forms a plane in direct-quadrature space of V_{Cd}, V_{Cq} . The steady-state based controller will use this information to calculate the exact solution to the steady-state power flow control problem.

III. CONTROLLER DESIGN

The two controllers here proposed use a model inverse to linearize and decouple control, while a small controller realizes zero steady state error in closed loop control. Dynamic and steady-state inverse controller differ only in the used model inverse. Only one power system parameter necessary for design of here proposed controllers, namely the L/r -ratio of the transmission line. Both controllers realize a first order system behavior when system model is valid.

A. Dynamic Inverse controller

The controllable part of active and reactive power flow was modeled in equation 9, and is repeated in matrix form in equation 13. For notation simplicity, matrix $A(s)$ is introduced in equation 12. Notice that $A(s) = \det A(s) \cdot A(s)^{-1}$.

$$A(s) = \begin{bmatrix} (L \cdot s + r) & \omega \cdot L \\ \omega \cdot L & -(L \cdot s + r) \end{bmatrix} \quad (12)$$

$$\begin{bmatrix} \Delta P(s) \\ \Delta Q(s) \end{bmatrix} = \frac{-V_{sd} \cdot A(s)}{\det A(s)} \cdot \begin{bmatrix} V_{cd}(s) \\ V_{cq}(s) \end{bmatrix} \quad (13)$$

The inverse of the power flow model in equation 13 is given in equation 15. This inverse could be used in an open-loop control system to calculate control signals $V_{Cd}(s), V_{Cq}(s)$ in function of reference active and reactive power flows $\Delta P_{ref}(s), \Delta Q_{ref}(s)$ as in equation 15. In Figure 4 a

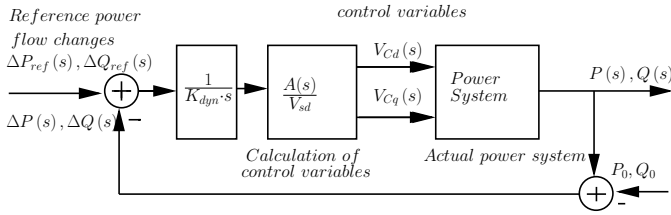


Fig. 5. Closed Loop Control structure, where $A(s)$ is used to linearize control and integrator $1/K_{dyn} \cdot s$ as controller. Actual Power system dynamics may differ from those modeled

schematic of such an open loop control system is shown. Calculating control variables by equation 15 is however not realizable, because of uncompensated zeroes in Laplace domain. Also, open loop control results in high sensitivity to modeling error.

$$\begin{aligned} P_{ref}(s) &= P_0(V_s, V_r) + \Delta P_{ref}(s) \\ Q_{ref}(s) &= Q_0(V_s, V_r) + \Delta Q_{ref}(s) \end{aligned} \quad (14)$$

$$\begin{bmatrix} V_{cd}(s) \\ V_{cq}(s) \end{bmatrix} = \frac{1}{V_{sd}} \cdot A(s) \cdot \begin{bmatrix} \Delta P_{ref}(s) \\ \Delta Q_{ref}(s) \end{bmatrix} \quad (15)$$

Changing the controller topology to feedback loop control, using the system model inverse to linearize control and adding a linear controller, in this case an integrator, to compensate zeroes in $A(s)$ results in calculation of control variables V_{cd}, V_{cq} as in equation 16. In Figure 5 a schematic of this closed loop control system is shown.

$$\begin{bmatrix} V_{cd}(s) \\ V_{cq}(s) \end{bmatrix} = \frac{1}{K_{dyn} \cdot s} \cdot \frac{A(s)}{V_{sd}} \cdot \begin{bmatrix} \Delta P_{ref}(s) - \Delta P(s) \\ \Delta Q_{ref}(s) - \Delta Q(s) \end{bmatrix} \quad (16)$$

The behavior of the controlled system can be estimated by combining the system model equation 13 and the calculation of the control variables 16. This result in a controlled system as in equation 17, or simplified as in equation 18.

$$\begin{bmatrix} \Delta P(s) \\ \Delta Q(s) \end{bmatrix} = \frac{1}{K_{dyn} \cdot s} \cdot \begin{bmatrix} \Delta P_{ref}(s) - \Delta P(s) \\ \Delta Q_{ref}(s) - \Delta Q(s) \end{bmatrix} \quad (17)$$

$$\begin{bmatrix} \Delta P(s) \\ \Delta Q(s) \end{bmatrix} = \frac{1}{K_{dyn} \cdot s + 1} \cdot \begin{bmatrix} \Delta P_{ref}(s) \\ \Delta Q_{ref}(s) \end{bmatrix} \quad (18)$$

The correct interpretation of equation 18 is that if the dynamic system model of equation 9 is a correct characterization of the actual power system, the dynamic inverse controller would realize a first order response to step changes in reference power flow $P_{ref}(s), Q_{ref}(s)$. Cross-coupling between active and reactive power flow $P(s), Q(s)$ is fully suppressed. This assumes that the power sources V_S, V_R demonstrate no dynamics and that control variables V_{cd}, V_{cq} stay within their range.

Using the same assumptions, the time constant of the controlled system can be chosen arbitrarily by changing parameter value $\frac{1}{K_{dyn}}$, which represents the open loop gain of the controlled system. For smaller values of K_{dyn} , and thus for smaller values of the controlled system's time constant, an equal step change in reference power flow will lead to bigger

control variable amplitudes V_{cd}, V_{cq} . Series inverter output voltage is limited. If control variable amplitudes reach series inverter output limits, applied control voltages are clipped. Compensation of the cross-coupled system dynamics is no longer possible, first order system characteristics are lost, and cross-coupling of active and reactive power flow control occurs.

The value of parameter K_{dyn} can be chosen arbitrarily. In case the actual values of line inductance and resistance L, r are not available, but the ratio L/r is, K_{dyn} can be used to compensate with the correct gain. This ratio L/r is commonly known for transmission lines [11].

This controller is constructed by four PI subcontrollers. Each of the two controller outputs is formed by a two different system dynamics. Each matrix element of $\frac{A(s)}{K_{dyn} \cdot s}$ will be formed by one PI controller. Two of these four will consist only of an integrator.

B. Steady-State Inverse controller

The steady-state controllable component of active and reactive power flow was calculated in equation 11, and is repeated in matrix form in equation 19. For ease of notation, $\omega \cdot L$ has been replaced with X_L . To enhance controller performance, the dominant time constant is incorporated in the steady state model. In other words, equation 19 is the solution to the steady-state power flow control problem, expanded with the dominant dynamics of the real system. This dominant time constant originates from the transmission line's inductance resistance ratio; $\tau = L/r$.

$$\begin{bmatrix} \Delta P \\ \Delta Q \end{bmatrix} = \frac{1}{\tau \cdot s + 1} \cdot \frac{V_{sd}}{r^2 + X_L^2} \cdot \begin{bmatrix} r & X_L \\ X_L & -r \end{bmatrix} \cdot \begin{bmatrix} V_{cd} \\ V_{cq} \end{bmatrix} \quad (19)$$

Design of the steady-state inverse controller is similar to the dynamic inverse controller and is therefore not given in extenso. An open loop controller using the inverse of the system in equation 19 would have an uncompensated zero. A closed loop controller using the system model inverse to linearize control and a linear controller, in this case an integrator, is formed in equation 20.

$$\begin{bmatrix} V_{cd} \\ V_{cq} \end{bmatrix} = \frac{\tau \cdot s + 1}{V_{sd} \cdot K_{ss} \cdot s} \cdot \begin{bmatrix} r & X_L \\ X_L & -r \end{bmatrix} \cdot \begin{bmatrix} \Delta P_{ref} - \Delta P \\ \Delta Q_{ref} - \Delta Q \end{bmatrix} \quad (20)$$

Similar as for the dynamic inverse controller, to estimate the behavior of the controlled system, equations 20 and 19 are combined, the total system reduces to 21.

$$\begin{bmatrix} \Delta P \\ \Delta Q \end{bmatrix} = \frac{1}{K_{ss} \cdot s + 1} \cdot \begin{bmatrix} \Delta P_{ref} \\ \Delta Q_{ref} \end{bmatrix} \quad (21)$$

Correct interpretation of equation 21 is that the steady-state inverse controller realizes a first order system response for steady state values, and steady-state cross-coupling is suppressed, but dynamic cross-coupling not. Similar remarks as for the dynamic inverse controller about K_{ss} , representing the controlled system time constant, are to be made here. K_{ss}

can be chosen arbitrarily; for decreasing values of K_{ss} , the system's time constant will decrease, but control variables' V_{Cd}, V_{Ca} amplitude will increase for equal step changes in reference power flow P_{ref}, Q_{ref} . The steady-state inverse controller depends only on the ratio L/r , where the exact values can be compensated by K_{ss} .

This controller is constructed by two PI subcontrollers. Each of the two controller outputs is formed by the main system dynamic $\frac{\tau \cdot s + 1}{K_{ss} \cdot s}$ multiplied by a sum of inputs. Therefore each output can be formed by one PI controller, making a total of two PI controllers..

IV. SIMULATION RESULTS

The proposed controllers are designed for a certain transmission line with known L/r -ratio. Both controllers are then tested in two different conditions. The first condition is the design condition. The transmission line has the same L/r -ratio and the switching frequency is infinite, sending and receiving end power sources are ideal; the controllers' theoretical performance is shown. The second condition introduces a limitation on switching frequency, a different transmission line with a different L/r -ratio, and a non-infinite receiving end power source. Assuming voltage support by the shunt convertor of the UPFC to the sending end power source, it is simulated as an infinite power source. In figure 6 the non-ideal transmission line is shown. By means of an intermediary load L_0, r_0 , the receiving end power source V_R appears as non-ideal for transmission line L_1, r_1 . Both a series impedance L_2, r_2 and a shunt impedance L_0, r_0 influence the apparent voltage and angle at the receiving end side of transmission line L_1, r_1 . The limited switching frequency introduces current and voltage harmonics into the system.. The connected transformer will act as a filter for these harmonics. This will reduce switching noise, but also control bandwidth. A second order filter is applied on measured power flow to visualize the filtering function of the transformer. System and controller parameters can be found in Appendix A. Inverter construction can be found in [12] and will not be discussed further.

Block waves with a frequency of 5 Hz are used as active and reactive power references. To clearly visualize the dynamic performance of the controllers, only the controlled part of the power flow is shown, both for the reference values $\Delta P_{ref}, \Delta Q_{ref}$ as for the measured values $\Delta P_{meas}, \Delta Q_{meas}$.

In Figure 7 the dynamic inverse controller is simulated in ideal design conditions. The response of controlled power flow to the block wave reference is indeed that of a first order system, as expected from equation 18. Cross-coupling between active and reactive power flow control is non-existent.

In Figure 8 the steady-state inverse controller is simulated in ideal design conditions. In the response of the controlled power flow to the block wave references, a resemblance to first order step response exists. There is no cross-coupling between active and reactive power flow for steady-state conditions, but dynamically there is. Every change in active or reactive power flow is answered by a smaller change in the other component. Oscillations occur, but are damped.

In ideal conditions, both the dynamic and the steady-state

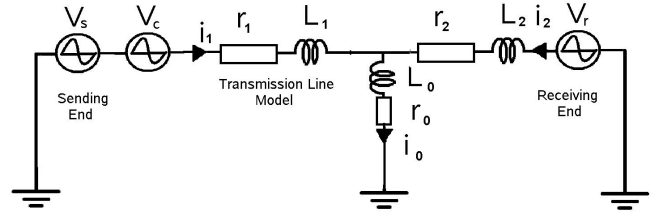


Fig. 6. Network to test controllers' performance and robustness

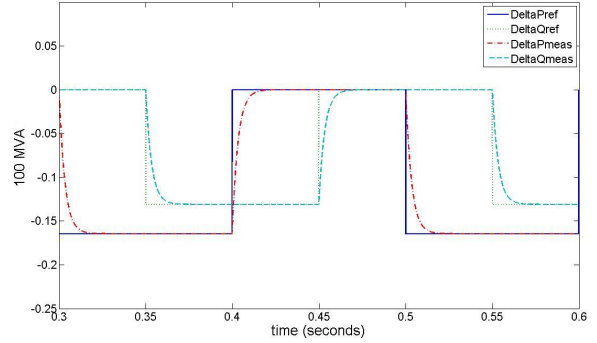


Fig. 7. $\Delta P, \Delta Q$ for Dynamic inverse controller in design conditions

inverse controller demonstrate sufficient control bandwidth to follow 5 Hz .

In Figures 9 and 10 the dynamic and steady-state inverse controller are tested in non-ideal conditions as explained before. The steady-state responses to power flow control references show that the controllers are both fairly insensitive to modeling errors (L/r -ratio), measurement noise (P_{meas}, Q_{meas}) and control noise V_C . Cross-coupling now appears also for the dynamic inverse controller, since its compensation is no longer adapted; ratio L/r of transmission line has changed. The filtering function of the transformer reduces the control bandwidth. This effect is stronger for the steady-state inverse controller than for the dynamic inverse controller.

Even though inter-area oscillations could not occur in the simulation model, the control bandwidth suggest that both controllers would be able to dampen them. The oscillation frequency of inter-area oscillations is typically $0.5 - 2 \text{ Hz}$. The limit of control bandwidth was not specifically measured in these simulations, yet the responses to the 5 Hz block wave reference signal proof that it is higher than 5 Hz .

V. CONCLUSION

The dynamic power flow equations of a transmission line equipped with a UPFC have been analyzed in this paper.

Two controllers, based on the dynamic and the steady-state power flow equations, are proposed. Simulations in ideal and non ideal conditions have proven the robustness of these controllers against modeling errors, measurement and control noise.

The controller based on the dynamic inverse demonstrates no cross-coupling of active and reactive power except when designed L/r -ratio differs from the actual value. The controller

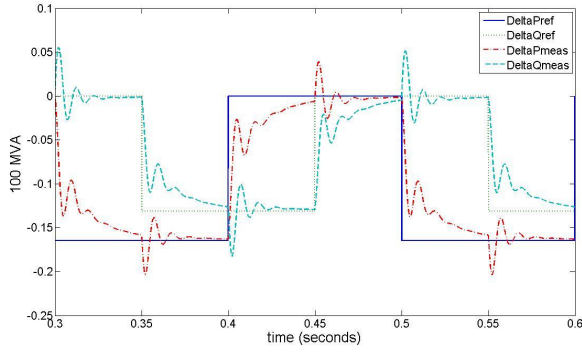


Fig. 8. $\Delta P, \Delta Q$ for Steady-state inverse controller in design conditions

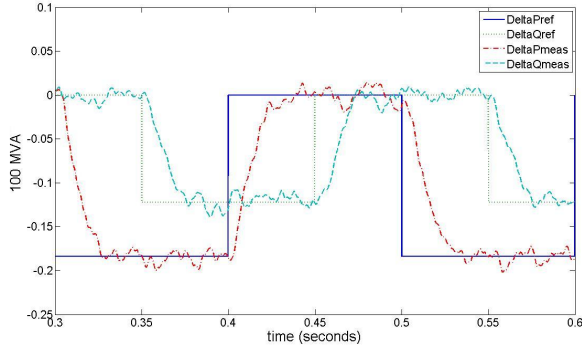


Fig. 9. $\Delta P, \Delta Q$ for Dynamic inverse controller in test conditions, switching frequency 1 kHz

based on the steady-state inverse demonstrates cross-coupling even in ideal conditions.

The proposed controllers' complexity is of the order of two or four PI controllers.

Both controllers realize a first order system behavior of the controlled system with arbitrary time constant. Both controllers' design only depends on the L/r -ratio of the line impedance.

Both proposed controllers allow inter-area oscillation damping.

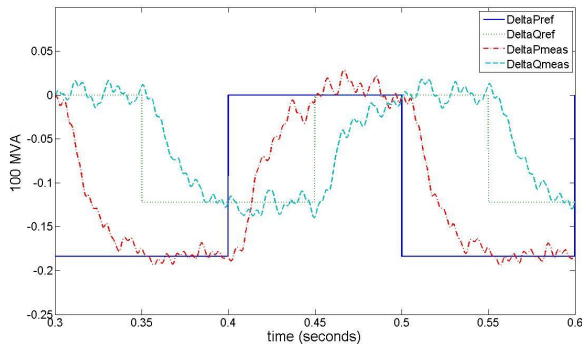


Fig. 10. $\Delta P, \Delta Q$ for Steady-state inverse controller in test conditions, switching frequency 1 kHz

APPENDIX A SIMULATION PARAMETERS

$$\begin{aligned}
 V_s &= \frac{150}{\sqrt{3}} \text{ kV} & V_r &= \frac{150}{\sqrt{3}} \text{ kV} & \omega &= 100 \cdot \pi & \delta &= \frac{\pi}{18} \text{ rad} \\
 X_L &= 33 \ \Omega & R &= 11 \ \Omega & K &= 0.01 & R_0 &= 1 \text{ k}\Omega \\
 X_1 &= 11.4362 \ \Omega & R_1 &= 4.3429 \ \Omega \\
 X_2 &= 22.1515 \ \Omega & R_2 &= 6.6217 \ \Omega \\
 V_{clim} &= 0.1 \cdot V_s
 \end{aligned}$$

Inverter capacitor voltage is limited to 4 kV and a connection transformer with ratio 15 was used. Transformer impedance assumed negligible in comparison to line impedance. Switching frequency of converters is limited to 1 kHz.

A second order filter is used with 200 Hz cut off frequency.

REFERENCES

- [1] S. D. Round, Q. Yu, L. E. Norum, and T. M. Undeland, "Performance of a unified power flow controller using a d-q control system," *Conference Publication Ac and Dc Power Transmission*, vol. 1, no. 423, 1996.
- [2] I. Papič, P. Žunko, D. Povh, and M. Weinhold, "Basic control of unified power flow controller," *IEEE Transactions on Industrial Electronics*, vol. 12, no. 4, Nov. 1997.
- [3] H. Fujita, Y. Watanabe, and H. Akagi, "Control and analysis of a unified power flow controller," *IEEE*, 1998.
- [4] H. Kim and H. Akagi, "The instantaneous power theory based on mapping matrices in three-phase four-wire systems," *IEEE*, 1997.
- [5] K. Sedraoui, K. Al-haddad, A. Chandra, and G. Olivier, "Versatile control strategy of the unified power flow controller," *IEEE*, 2000.
- [6] C. Yam and M. Haque, "A svd based controller of upfc for power flow control," *Electric Power Systems Research*, no. 70, pp. 79–84, 2004.
- [7] H. Wang and Q. Wu, "Multivariable design of a multiple-functional unified power flow controller," *IEEE*, 2000.
- [8] H.F. Wang, "Damping function of unified power flow controller," *IEE Proceedings Gener. Transm. Distrib.*, vol. 146, no. 1, Jan. 1999.
- [9] N. Tambey and P. M. L. Kothari, "Unified power flow controller (upfc) based damping controllers for damping low frequency oscillations in a power system," *IE journal EL*, vol. 84, June 2003.
- [10] H. Wang, "A unified model for the analysis of facts devices in damping power system oscillations-partiii: Unified power flow controller," *IEEE Transaction on Power Delivery*, vol. 15, no. 3, July 2000.
- [11] D. van Dommelen, *Productie, transport en distributie van elektriciteit*. Brusselsestraat 153, 3000 LEUVEN, BELGIUM: Uitgeverij Acco, 2001.
- [12] J. F. Silva, "Conversão multinível em electrónica de potência," Dec. 2001.